DEFECT DETECTION LIMITS FOR ADDITIVELY MANUFACTURED PARTS USING CURRENT THERMOGRAPHY TECHNIQUES

Nicholas J. Wallace, Matthew R. Jones, Nathan B. Crane

Brigham Young University
Ira A. Fulton College of Engineering,
Provo, Utah 84602

ABSTRACT

Additive manufacturing (AM) will support NASA in their moon and mars missions by reducing the amount of redundant equipment carried into space and by providing crew members with the flexibility to design and create parts as needed. The ability to monitor the quality of these additively manufactured parts is critical, especially when using recycled or in-situ materials as NASA plans to do. This project assesses the possibility of detecting small, shallow AM defects with existing active thermography techniques. An axisymmetric, numerical model was created in COMSOL to simulate the heat transfer within AM structures during active thermography. The effects of surface convection, heat conduction through the subsurface defect, and radiative in-depth absorption were included in the model. The simulation results estimate the minimum detectable defect diameter for a given defect depth using a common thermography technique. Additionally, the data demonstrates conditions for which 1D thermography models may be applied to 3D systems.

NOMENCLATURE

|	
AM	Additive manufacturing
FFF	Fused filament fabrication
T_c	Temperature contrast between a defective and non-defective region
Z_d	Defect depth
α	Thermal diffusivity
t	Time
D_d	Defect diameter
h_d	Defect height
$q_o^{"}$	Incident heat flux
q_{conv}	Convective heat loss
h_c	Cylinder height
r_c	Cylinder radius
$t_{Tc\prime}$	Time at which the derivative of the temperature contrast peaks
A_R	Aspect ratio; (D_d/Z_d)
κ_λ	Spectral absorption coefficient
β	Transmissivity of a singular light ray passing through the polymer above the subsurface pocket of air
R	Reflectivity
σ	Stephan-Boltzmann constant
$q_{rad,defect}^{"}$	Radiative heat flux through the defect
$q_{cond,defect}^{"}$	Conductive heat flux through the defect
k_{air}	Thermal conductivity of air
Γ	Ratio of $t_{Tc\prime}$ from the numerical data divided by $t_{Tc\prime}$ from the analytical model given in Eq. (1)

1. INTRODUCTION

NASA has allocated extensive time and money into additive manufacturing [AM] research [1, 2]. The flexibility to adapt designs and create parts and supplies as needed could be critical for crew members who live for extended periods in space, on the moon, or on mars [3]. In addition, relying on AM technologies could reduce payload weight by eliminating redundant equipment carried into space. This is especially true if material is recycled or mined on the moon or mars for AM fabrication [1, 4]. However, utilizing recycled material or in-situ resources could be unpredictable, and result in AM structures whose properties are not accurately known.

Using non-ideal materials during AM can also increase defect formation [5, 6]. Figure 1 demonstrates three different types of AM defects that are common in fused filament fabrication (FFF). First, imperfections in the filament can cause small entrapments of air as indicated by letter A. These voids are sometimes present in the purchased filament even before printing. Second, gaps in the matrix (letter B in Figure 1) can be caused by poor printing parameters, uneven deposition of material, and uneven filament diameters. Third, poor adhesion of a printed layer to the previous layer can lead to separation known as delamination (Letter C of Figure 1). Delamination is often the

source and mode of failure when subjecting FFF parts to a load, whereas the other voids indicated by letters A and B of Figure 1 merely act as stress concentrators which initiate delamination [7-9].
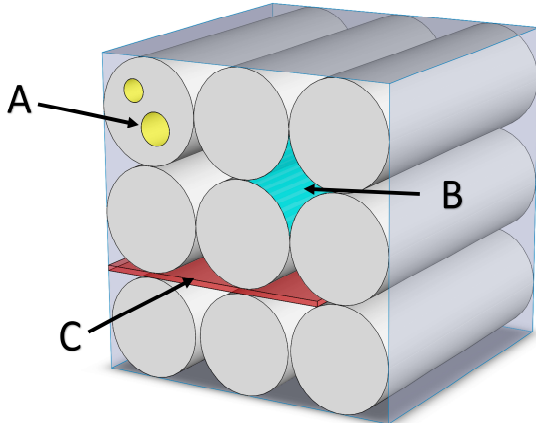

Figure 1: THREE DIFFERENT TYPES OF DEFECTS IN FFF. A) VOIDS WITHIN THE FILAMENT. B) VOIDS IN THE MATRIX. C) SEPARATION OF PRINTED LAYERS (DELAMINATION).

In all additive manufacturing quality assurance is critical, but especially in space applications where resources are limited, and failure could result in catastrophe. Common AM quality assurance techniques include: scanning electron microscopy, X-ray diffraction, acoustic emission detection, and ultrasonic testing [10-12]. However, these techniques can be expensive, bulky, and or require a significant amount of time to perform measurements. The hypothesis of this research is that NASA can ensure the quality of their additively manufactured parts through a non-destructive technique called active thermography.

Active thermography is performed by irradiating an object's surface and measuring the transient surface temperature as illustrated in Figure 1 [13]. Because the thermophysical properties of defects differ from the properties of non-defective regions, heat transfer models can be used to reveal the location of flaws and to approximate their depth or size [14-19]. Preliminary research has suggested that active thermography could be applied to the materials and conditions common in AM [20-22]. However, there are two questions which need to be addressed before understanding if active thermography is the best option for quality assurance of NASA's AM applications.

First, it is unknown if the small defects shown in Figure 1, letters A and B, are detectable via active thermography. Even small pores on the order of 100 µm can have significant effects on the integrity of the final part [23, 24]. Therefore, the detection threshold of active thermography needs to be investigated to ensure its applicability in AM. Second, the polymeric materials commonly used in FFF have relatively low absorption coefficients. Previous research through the Utah Nasa Space

Grant has shown how these low spectral absorption coefficients can significantly affect the transient temperature profiles used in active thermography [13]. The effects of radiative in-depth absorption on AM defect detection will need to be investigated, especially when analyzing shallow defects which form within the spectral absorption depth of the material.
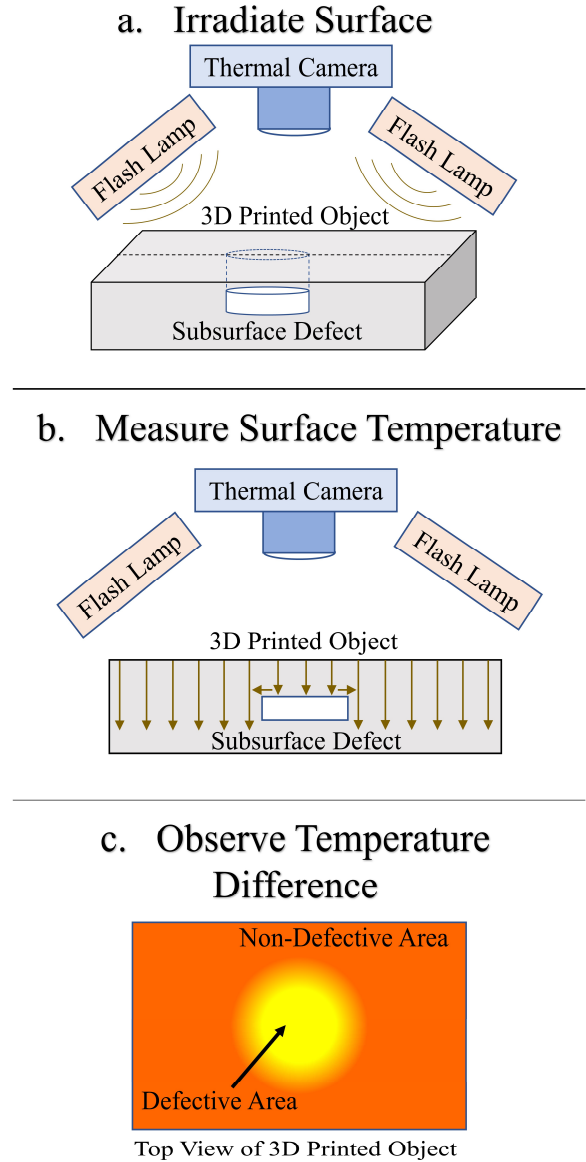
FIGURE 2: THERMAL RESPONSE OF DEFECTIVE AND NON-DEFECTIVE AREAS AFTER BEING IRRADIATED BY A FLASH LAMP. THE LINES IN (B) REPRESENT A THERMAL WAVE PROPAGATING THROUGH THE OBJECT. AREAS WITH LOW THERMAL CONDUCTIVITY OBSTRUCT THE PROPAGATION OF SUCH WAVES AND CAUSE HIGHER SURFACE TEMPERATURES [13].

This research will investigate the detection threshold of active thermography in AM as a function of defect depth and diameter. Numerical models will be used to simulate the heat

transfer during active thermography around and through subsurface pockets of air embedded in AM polymers. In addition, the effects of non-ideal conditions (radiative in-depth absorption, surface convection, 1D heat transfer approximations) commonly used in active thermography models will be analyzed, and their effects on detection limits will be evaluated.

2. MATERIALS AND METHODS

The detection threshold will be determined with respect to a commonly used thermography model developed by Ringermacher et al. [25]. This model is an adaptation of the thermal diffusivity measurement technique developed by Parker et al. in the 60's [26]. Ringermacher uses the time at which the maximum of the derivative of the temperature contrast, T_c, occurs to predict the defect depth as shown in Eq. (1). T_c is defined as the difference between surface temperature directly above a flaw and the surface temperature of a non-defective region (an area unaffected by defects or boundaries). In Eq. (1), Z_d is the defect depth (the distance from the surface of the object to the top surface of the defect), α is the thermal diffusivity of the material in which the defect is embedded, and t is the time.

$$time \ of \ max\left(\frac{dT_c}{dt}\right) = t_{Tc'} \cong \frac{3.64 * Z_d^2}{\pi^2 * \alpha} \quad (1)$$

Although commonly used, this model has many limiting assumptions. This model assumes that the heat transfer is one dimensional, that the irradiative pulse is instantaneous, and that the radiation is absorbed in an infinitesimal layer on the surface of the object. In addition, it assumes that the boundaries of the defect and of the object in which the defect is embedded are adiabatic. Deviations from these ideal conditions will affect the accuracy of the results obtained.

The following sections will describe how a numerical model was created to investigate the geometric limits of the model shown in Eq. (1) and to determine how non-ideal conditions affect its results.

2.1 Numerical Modeling

COMSOL multiphysics software was used to create an axisymmetric, numerical model. Figure 3 shows the basic geometries and boundary conditions used. The simulation swept through a large number of defect diameters (D_d) at two discrete defect depths (Z_d) in order to mimic defect geometries and locations typical to AM [5, 6]. The defect height (h_d) was set to a common layer height for many AM processes (50 µm). A short pulse ($q_o^"$) irradiated the top surface of the model for the duration of a single time step (.0001 sec) after which convective cooling occurred (q_{conv}). A typical convection coefficient was selected for free convection (10 W/(m^2 K)). The value of $q_o^"$ was determined by running multiple simulations and observing if the maximum

surface temperature exceeded the glass transitional temperature of the polymer being analyzed (Nylon 12). The thermal conductivity, specific heat capacity, density, and spectral absorption coefficient of Nylon 12 used in the model were 0.260 (W/mK), 1640 (J/kg K), 990 (kg/m^3), and 0.026 (1/µm) respectively [13, 21, 27].

The cylinder was thermally insulated on all surfaces expect for the top where convective cooling occurred. During some of the simulations the boundaries surrounding the defect were thermally insulated, whereas during others these adiabatic boundaries were removed, and heat was permitted to conduct through the flaw. This was done to investigate the effects of removing the ideal conditions assumed when deriving Eq. (1) [25]. The cylinder's total width changed as a function of the defect diameter to ensure that the "sound" area was unaffected by the temperature change above the defect.
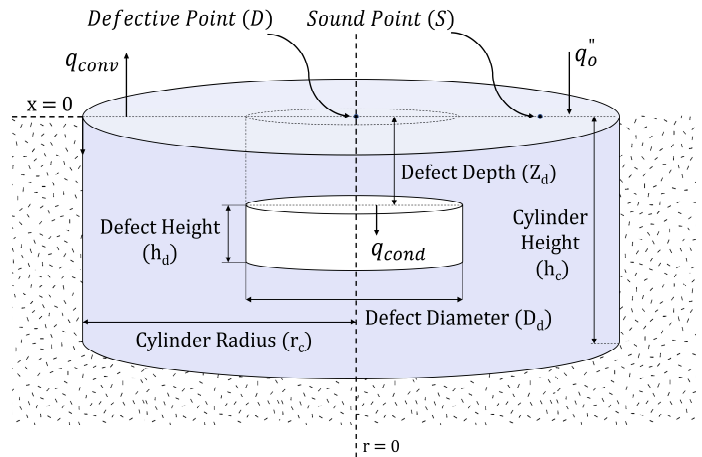
Figure 3: BASIC GEOMETRY USED IN THE AXISYMMETRIC COMSOL MODEL. A CONVECTIVE BOUNDARY DEFINED THE TOP SURFACE, WHEREAS ALL OTHER SIDES WERE INSULATED.

2.2 Convergence

A convergence study was performed on the numerical model to verify adequate mesh refinement and time stepping. The critical time shown in Eq. (1) was used to verify that the model had fully converged. Model convergence on this derivative parameter ensured full convergence when also calculating the temperature contrast, T_c. The mesh element size was halved until the difference in $t_{Tc'}$ between iterations was less than 0.002 seconds.

The time step was decreased by a factor of ten until the difference in $t_{Tc'}$ between iterations was less than 0.002 seconds. The "relative tolerance" was also decreased by a factor of ten until the same convergence criteria was met. COMSOL uses to the relative tolerance to describe how small the residuals need to be between iterations before advancing to the next time step.

TABLE 1: FINAL SIMULATION SETTINGS OF CONVERGED MODEL

Time Step (sec)	Number of Mesh Elements	Relative Tolerance	Cylinder Height (m): h_c	Cylinder Radius (m): r_c	Defect Height (μm): h_d	Distance from point S to point D (m)	Power Input (J/m^2): E
0.0001	132,871	$1 * 10^{-7}$	0.02	$\frac{D_d}{2} + 0.038$	50	$\frac{D_d}{2} + 0.017$	2500

The "sound region", indicated by point S in Figure 3, was also verified by running two simulations with different defect geometries. The defect aspect ratio ($A_R = D_d/Z_d$) was increased from a value of one to a value of twenty between the two simulations, while all other parameters where kept the same. The difference in surface temperatures between these two simulations never exceeded 0.0005K. Therefore, the location was unaffected by the increased temperature above the defect. The final simulation settings of the converged model are given in Table 1.

2.3 Modeling Non-Ideal Conditions

Eq. (1) assumes that the heat transfer is one dimensional, that the irradiative pulse is instantaneous, and that the radiation is absorbed in an infinitesimal layer on the surface of the object. In addition, it assumes that all boundaries are adiabatic. The following paragraphs describe how the numerical model was used to investigate the effects of deviating from these ideal conditions.
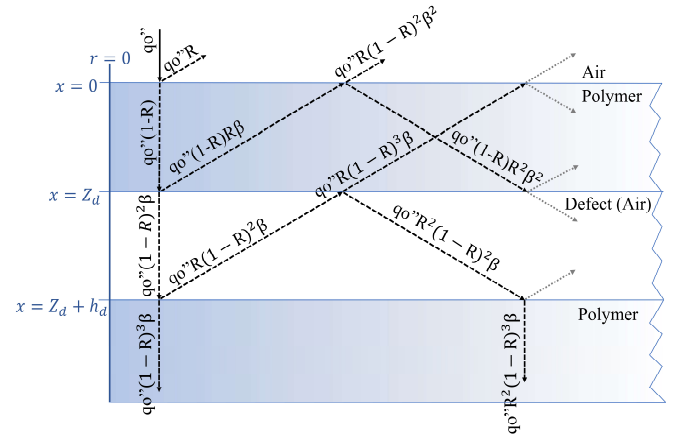
Traditionally, active thermography models have assumed that irradiation is absorbed in an infinitesimal layer at the object's surface [14, 15, 18-22, 25, 26]. For materials with relatively large spectral absorption coefficients (κ_λ), this approximation has yielded good results. The spectral absorption coefficient describes the exponential rate at which spectral intensity decreases as it propagates into a material [28]. However, the polymers used in AM have relatively low spectral absorption coefficients. This increased absorption depth can significantly alter the transient surface temperature used during active thermography [13].

Figure 4 illustrates the increased modeling complexity when spectral in-depth absorption is included. If the subsurface flaw resides within the spectral absorption depth of the material, the irradiation is either transmitted through or reflected off the polymer-air interfaces shown. In Figure 4, the material is assumed to be non-scattering. The reflectivity of the material is represented by R, and the flux of the irradiative pulse (W/m^2) is represented by q_o". β describes the transmissivity of a single ray passing through the polymer above the subsurface pocket of air and is defined by Eq. (2).

$$\beta = e^{-\kappa_\lambda Z_d} \qquad (2)$$

The internal reflections and transmissions directed into the polymer at the three polymer-air interfaces (where x equals 0, Z_d, and $Z_d + h_d$) were summed together. Because the reflectivity of

the selected material is relatively small (~.05 [13]), it was assumed that any term multiplied by R^4 would be negligible; therefore, the internal reflection and transmission terms were extended until an R^4 was present in each. These terms were manually added in the COMSOL model by creating "analytical expressions" with domains that were restricted to the area directly above or below the defect. Absorption of the irradiative pulse outside the defective area was defined similar to Eq. (1). with the replacement of Z_d with x.

Figure 4: MODELING REFLECTED IRRADIATION WITHIN THE OBJECT. NOTE THAT THE INCIDENT RADIATION, REFLECTIONS, AND TRANSMISSIONS ARE ALL NORMAL TO THE TOP SURFACE.

In most active thermography models, defects are considered to have adiabatic boundaries [14, 15, 18-20, 25, 26]. This might not be an accurate assumption under all conditions, especially when analyzing materials whose thermal conductivity is closer to that of air. To evaluate the impact of adiabatic defect assumptions, heat was permitted to conduct through the flaw during some of the simulations.

Free convection was not included within the subsurface, cylindrical pocket of air. This was because the hotter top surface resulted in a stable temperature gradient [29]. If the following approximations are made: a view factor of one between the top and bottom surfaces of the defect, a defect height of 50µm, a temperature difference of 10 K, and a surface emissivity of 1; then the ratio of radiative to conductive heat flux through the defect can be approximated by Eq. (3). In this equation, σ is Stephan-Boltzman's constant, k_{air} is the thermal conductivity of air, $T_{x=Z_d}$ is the temperature of the top surface of the defect, and $T_{x=Z_d+h_d}$ is the temperature of bottom surface of the defect. The

ratio of radiative to conductive heat flux through the flaw under these conditions is approximately 0.012. From these basic calculations, radiation exchange between the top and bottom surfaces of the defect was considered negligible and was therefore excluded from the model.

$$\frac{q''_{rad,defect}}{q''_{cond,defect}} \approx \frac{\sigma(T^4_{x=Z_d} - T^4_{x=Z_d+h_d})h_d}{k_{air}(T_{x=Z_d} - T_{x=Z_d+h_d})} \quad (3)$$

3. RESULTS

The results from the numerical simulation were non-dimensionalized using the Eqs. (4) and (5). Eq. (5) represents the ratio between the time at which the derivative of the temperature contrast peaks from the numerical data divided by the same time approximated by the model presented in Eq. (1). Thus, when the data reaches a value of 1, the conditions are considered ideal, and Eq. (1) accurately predicts the depth of a defect.

$$A_R = \frac{D_d}{Z_d} \quad (4)$$

$$\Gamma = \frac{t_{T'_c} \, (from \, numerical \, simulation)}{t_{T'_c} \, (from \, Eq. \, (1))} \quad (5)$$

Figures 5 and 6 illustrate the non-dimensionalized time and temperature contrast versus aspect ratio respectively. The results were retrieved by sweeping through a large range of defect diameters at two specific depths (100 and 200 μm). Data labeled "non-ideal" in the legend indicates that in-depth absorption, conduction through the subsurface flaw, and convection from the top surface of the object were included in the model.

4. CONCLUSION AND DISCUSSION

The detection limit was determined by considering the defect diameter at which Eq. (1) would yield accurate results. Because Eq. (1) assumes highly idealized conditions, including 1D heat transfer, these results indicate what defect diameter is required for the 3D system to behave one-dimensionally during the measurement period. As can be seen in Figure 5, the aspect ratio for which a 3D system will behave as a 1D system (assuming adiabatic boundaries around the flaw, no convection from the surface of the object, and no radiative in-depth absorption) is approximately 6. However, using Eq. (1) to approximate the depth of a defect with an aspect ratio of 4 would still yield reasonably accurate results (<10% error) for the ideal conditions mentioned previously.
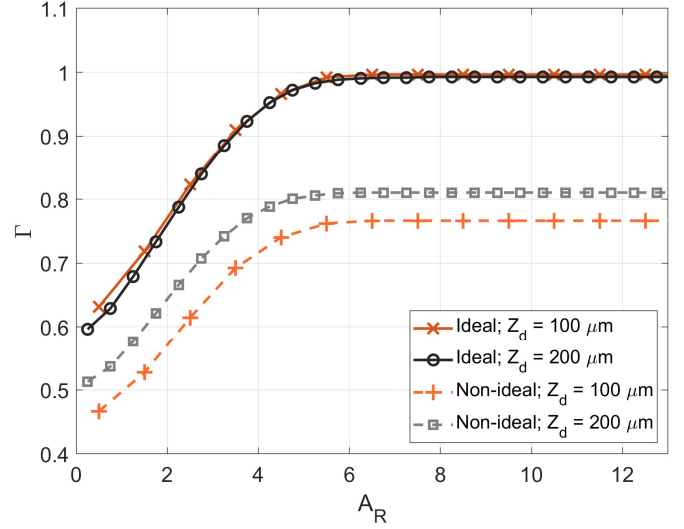
Figure 5: THE RATIO BETWEEN THE TIMES AT WHICH THE DERIVATIVE OF THE TEMPERATURE CONTRAST PEAKS FROM THE NUMERICAL DATA DIVIDED BY THE SAME CRITICAL TIMES APPROXIMATED BY THE MODEL IN EQ. (1), Γ, AS A FUNCTION OF THE DEFECT ASPECT RATIO, A_R.
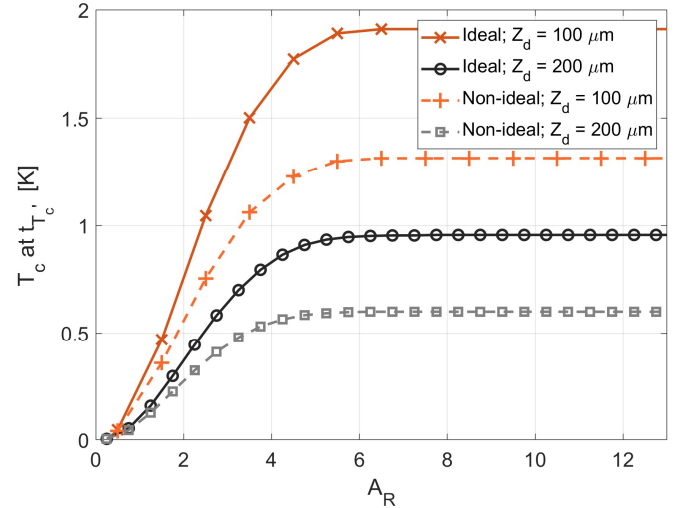
Figure 6: TEMPERATURE CONTRAST, T_c, AT THE CRITICAL TIMES SHOWN IN EQ. (1), $t_{T_{c'}}$, VERSUS DEFECT ASPECT RATIO, A_R.

Figure 5 also indicates that the Eq. (1) is not as accurate (error > 20%) when approximating the depth of defects in systems that have the non-ideal conditions mentioned previously. In fact, the non-ideal data never approaches a value of 1, despite the large aspect ratios being analyzed. This is to be expected, because including convective heat loss and in-depth absorption deviates from the ideal conditions used to derive Eq. (1). It is interesting to note that the non-ideal data plateaus at the same aspect ratio as the ideal data. This implies that there is physical significance with respect to this aspect ratio value.

Further research is needed to create an analytical model to describe this phenomenon.

Figure 6 demonstrates that the temperature contrast at these critical times are higher than the noise of a typical thermal camera (~.2K). Thus, detection and analysis of these small defects is possible. However, this study did not consider the spatial resolution of typical cameras, nor the frame rate required to capture the transient nature of the temperature profile. Future work is needed to investigate these spatial resolution and frame rate limitations.

The detection limits provided are useful in understanding the applicability of active thermography in AM processes. The implementation of active thermography is relatively simple, cheap, and fast when compared to other AM quality assurance methods as discussed previously. As NASA investigates AM to reduce payload weight, and provide flexibility for crew members in space, active thermography shows potential in providing the quality assurance needed to ensure parts created from recycled and or in-situ material are functional.

ACKNOWLEDGEMENTS

REFERENCES

1. Harbaugh, J., *Refabricator to Recycle, Reuse Plastic Installed on Space Station.* 2019.
2. Skelly, C.P., M. *NASA Looks to Advance 3D Printing Construction Systems for the Moon and Mars*. 2020.
3. Dunbar, B., *Moon to Mars Overview.* 2019.
4. Chawla, K., Singh, R., Singh, J., *On recyclability of thermoplastic ABS polymer as fused filament for FDM technique of additive manufacturing.* World Journal of Engineering, 2021.
5. Wickramasinghe, S., Do, T., Tran, P., *FDM-Based 3D Printing of Polymer and Associated Composite: A Review on Mechanical Properties, Defects and Treatments.* Polymers, 2020. **12**(7): p. 1529.
6. Vyavahare, S., et al., *Fused deposition modelling: a review.* Rapid Prototyping Journal, 2020. **26**(1): p. 176-201.
7. Oztan, C., et al., *Microstructure and mechanical properties of three dimensional-printed continuous fiber composites.* Journal of Composite Materials, 2019. **53**(2): p. 271-280.
8. Rodríguez, J., Thomas, J., Renaud, J., *Mechanical behavior of acrylonitrile butadiene styrene (ABS) fused deposition materials. Experimental investigation.* Rapid Prototyping Journal, 2001.
9. Dong, C., *Effects of Process-Induced Voids on the Properties of Fibre Reinforced Composites.* Journal of Materials Science & Technology, 2016. **32**(7): p. 597-604.
10. Li, Y., et al., *In-Situ Monitoring and Diagnosing for Fused Filament Fabrication Process Based on Vibration Sensors.* Sensors, 2019. **19**(11): p. 2589.
11. Shmueli, Y., et al., *In-situ X-ray scattering study of isotactic polypropylene/graphene nanocomposites under shear during fused deposition modeling 3D printing.* Composites Science and Technology, 2020. **196**: p. 108227.
12. Cummings, I., et al., *In-Process Ultrasonic Inspection of Additive Manufactured Parts*. 2016, Springer International Publishing. p. 235-247.
13. Wallace, N., Jones, M., Crane, N., *Spectral Absorption Coefficient of Additive Manufacturing Polymers.* USU Digital Commons 2020.
14. Sun, J.G., *Analysis of pulsed thermography methods for defect depth prediction.* Journal of Heat Transfer-Transactions of the Asme, 2006. **128**(4): p. 329-338.
15. Sun, J.G., *Quantitative Three-Dimensional Imaging of Heterogeneous Materials by Thermal Tomography.* Journal of Heat Transfer-Transactions of the Asme, 2016. **138**(11).
16. Busse, G., Wu, D., Karpen, W., *Thermal Wave Imaging with Phase Sensitive Modulated Thermography.* Journal of Applied Physics, 1992. **71**(8): p. 3962-3965.
17. Lau, S., Almond, D., Milne, J., *A quantitative analysis of pulsed video thermography.* NDT & E International, 1991. **24**(4): p. 195-202.
18. Maldague, X., Marinetti, S., *Pulse phase infrared thermograph.* Journal of Applied Physics, 1996. **79**(2694).
19. Maldague, X., Galmiche, F., Ziadi, A., *Advances in pulsed phase thermography.* Infrared Physics & Technology, 2002. **43**(3-5): p. 175-181.
20. Metz, C., Franz, P., Fischer, C., Wachtendorf, V., Maierhofer, C. , *Active thermography for quality assurance of 3D-printed polymer structures* 14th Quantitative InfraRed Thermography Conference, 2018.
21. Pierce, J., Crane, N., *Impact of pulse length on the accuracy of defect depth measurements in pulse thermography.* Journal of Heat Transfer-Transactions of the Asme, 2019. **141**(4).
22. Pierce, J., Crane, N., *Preliminary Nondestructive Testing Analysis on 3d Printed Structure Using Pulsed Thermography.* Proceedings of the Asme International Mechanical Engineering Congress and Exposition, 2017 Vol 8, 2018.
23. Sanaeia , N., Fatemiab, A., Phanc, N., *Defect characteristics and analysis of their variability in metal L-PBF additive manufacturing.* Materials & Design, 2019. **182**.

24. Yadollahi, A., Shamsaei, N., Thompson, N., Elwany A., Bian, L., *Effects of building orientation and heat treatment on fatigue behavior of selective laser melted 17-4 PH stainless steel.* International Journal of Fatigue, 2016. **94**((2017)): p. 218–235.

25. Ringermacher, H., Archacki, R., Veronesi, W., *Nondestructive Testing: Transient Depth Thermography*, in *U.S. Patent*. 1998: USA.

26. Parker, W., Jenkins, R., Abbott, G., Butler, C., *Flash Method of Determining Thermal Diffusivity, Heat Capacity, and Thermal Conductivity.* Journal of Applied Physics, 1961. **32**(9): p. 1679-&.

27. Yuan, M., Bourell, D., Diller, T., *Thermal Conductivity Measurements of Polyamide 12.* Laboratory for Freeform Fabrication, Mechanical Engineering Department The University of Texas at Austin, 2011.

28. Modest, M.F., *Radiative Heat Transfer.* New York: Academic Press, 2013.

29. Bergman, T., Adrienne, L., Incropera, F., Dewitt D., *Fundamentals of Heat and Mass Transfer, Seventh Edition*. 2008. 622.